Liu *et al.*
Chinese Journal of Mechanical Engineering (2022) 35:144
https://doi.org/10.1186/s10033-022-00816-y

Chinese Journal of Mechanical Engineering

ORIGINAL ARTICLE

Open Access

MPC-Based Coordinated Control of Gear Shifting Process for a Power-split Hybrid Electric Bus with a Clutchless AMT

Tong Liu, Xiaohua Zeng* and Dafeng Song

Abstract

Two-speed clutchless automated manual transmission (AMT) has been widely implemented in electric vehicles for its simple structure and low cost. In contrast, due to the complex response characteristics of powertrain, utilizing clutchless AMT in a hybrid power system comes with complex coordination control problems. In order to address these issues, a power-split hybrid electric bus with two-speed clutchless AMT is studied in this paper, and a coordinated control method based on model predictive control (MPC) is used in gear shifting control strategy (GSCS) to improve gear shifting quality and reduce system jerk. First, the dynamic model of power sources and other main powertrain components including a single planetary gear set and AMT are established on the basis of data-driven and mechanism modeling methods. Second, the GSCS is put forward using the segmented control idea, and the shifting process is divided into five phases, including (I) unloading of drive motor, (II) shifting to neutral gear, (III) active speed synchronization by drive motor, (IV) engaging to new gear, and (V) resuming the drive motor's power, among which the phases I and V have evident impact on the system jerk. Then, the MPC-based control method is adopted for these phases, and the fast compensation of driving torque is realized by combining the prediction model and quadratic programming method. The simulation results show that the proposed GSCS can effectively reduce shift jerk and improve driving comfort. This research proposes a coordinated control strategy of two-speed clutchless AMT, which can effectively improve the smoothness of gear shifting and provides a reference for the application of two speed clutchless AMT in power-split hybrid powertrains.

Keywords: Power-split hybrid electric bus, Shift jerk, Model predictive control

1 Introduction

With the aggravation of energy crisis, hybrid electric vehicle (HEV) has attracted increasing attention due to its high fuel economy and low emission. In various hybrid powertrains with different structure forms, the power-split hybrid system is widely used because the engine is decoupled from the vehicle speed and required driving torque. Thus, continuous adjustment of the engine speed and optimization control of the engine operating point are realized [1–3]. Considering the technical level, cost, and other factors, the mainstream of the power coupling device in power-split HEV is single planetary gear set (SPGS), and some dual planetary systems are only variants of the former. At present, the research on the control theory of single planetary system is relatively mature and has achieved good economic and social benefits. However, some problems such as parasitic power after mechanical point, high temperature at high speed of motor, and weakness of dynamic property in pure electric mode are present. To overcome these shortcomings, automatic mechanical transmission (AMT) can be added to the powertrain, and the drive motor transmission ratio can be changed in accordance with the power and fuel economic requirement to achieve the ideal driving

*Correspondence: zengxh@jlu.edu.cn

State Key Laboratory of Automotive Simulation and Control, Jilin University, Changchun 130025, China

© The Author(s) 2022. **Open Access** This article is licensed under a Creative Commons Attribution 4.0 International License, which permits use, sharing, adaptation, distribution and reproduction in any medium or format, as long as you give appropriate credit to the original author(s) and the source, provide a link to the Creative Commons licence, and indicate if changes were made. The images or other third party material in this article are included in the article's Creative Commons licence, unless indicated otherwise in a credit line to the material. If material is not included in the article's Creative Commons licence and your intended use is not permitted by statutory regulation or exceeds the permitted use, you will need to obtain permission directly from the copyright holder. To view a copy of this licence, visit http://creativecommons.org/licenses/by/4.0/.

power and economic performance of the vehicle [4, 5]. However, adding new components are easy to increase the complexity and difficulty of control. Especially during gear shifting, the power interruption easily results in system jerk and significantly impacts driving comfort.

At present, studies on the shifting process of HEV equipped with AMT are abundant. Glielmo et al. proposed a hierarchical method for different AMT operating phases based on cascaded and decoupled speed and torque control loops [6]. Jo et al. [7] raised a control strategy to reduce the synchronizing torque of synchronizer and clutch by controlling the torques and speeds of the engine and motor. Xie et al. [8] exploited a control strategy based on pontryagin's minimum principle to realize a predictive controller in a receding horizon mode for a plug-in hybrid electric vehicle equipped with an AMT. Li et al. [9] proposed coordinated control of the combined clutch and the motor and adopted linear quadratic optimal control to optimize the shifting process. This method significantly reduced the shift jerk and sliding friction work compared with the pure clutch control. These methods achieve the optimal control of gear shifting by integrated control of clutch and power source. However, the control characteristics of clutch are complex, and achieving accurate control effect is difficult [10]. In practical application, substantial experimental work is needed to extract control rules, which restrict the application of these methods.

Some scholars have proposed clutchless shifting control methods, considering the control difficulty and purchase cost of clutch. Liao and Zhang studied the problems of synchronizer wear, clutch wear, and long power interruption time in the shifting process of a parallel hybrid electric vehicle; they improved the shift quality and shortened the shift time by coordinating and controlling the engine and motors [11]. Wang proposed a combined control algorithm for engine control during shift without the use of clutch by adjusting the throttle opening, ignition timing, and fuel injection; the simulation results are excellent. Yu et al. analyzed the parameters affecting the gear shifting time, component life, and gear shifting jerk in different transient states during the shifting process, and then proposed a dynamic coordinated control strategy of the motor, engine, and actuators [11]. The results show that the proposed control strategy can improve the gear shifting quality. Pettersson et al. proposed a novel idea without using clutch to realize gear shifting and extend the service life of the clutch. This approach realized fast and smooth shift by controlling the torque of the engine [12]. Zhong realized the precise control of the engine by combining the feed-forward, bang-bang, and PID control and proposed a control method based on linear quadratic regulator to control the AMT actuator. The experiment results show that the coordinated control algorithm proposed by Zhong can achieve shifting control without the use of the clutch. This approach improves driving comfort significantly and extends the service life of the clutch [13]. The proposed control method confirms that a good shift effect can be achieved through active control of motor and engine without clutch. However, their powertrain structures are simple, and the control algorithms are difficult to apply to more complex powertrains, especially planetary gear system with dual motors, in which, the driving torque can be compensated by controlling multiple power sources to reduce the shift jerk.

The response characteristics of the engine, motor and other components of hybrid power system are obviously different [14]. Thus, the characteristics of each component should be fully understood to achieve good shifting control. Model predictive control (MPC) is an effective control method and is widely used in hybrid powertrains [15, 16]. Zeng et al. designed a state feedback controller based on MPC theory to eliminate system jerk during mode shifting of power-split hybrid electric buses (PS-HEBs). The robustness of control effect can be better ensured through the online rolling optimization by combining the feedback control and the predictive model [17, 18]. Qi et al. developed an economic MPC-based transient control strategy to further improve the accurate reference tracking performance of a compound power-split system, which achieved a better response, as well as the efficiency of the transmission system [19]. The accuracy of the control-oriented model and the real-time performance should be guaranteed to ensure the control effect of the MPC-based dynamic coordination control strategy in engineering application [20]. However, few researchers apply MPC to shifting control of a clutchless AMT.

For a hybrid powertrain equipped with a clutchless transmission, the main factors affecting the system jerk during gear shifting are the torque of engine and motor [21, 22]. The difference in the response characteristics of engine and motor could cause significant torque fluctuations when shifting, especially with high torque. And the advantages of fast response and high control accuracy of the motor can be fully utilized to compensate torque changes in time. At present, researches on the torque response characteristics of engine and motor are quite sufficient [23, 24]. By establishing the transient torque response model of power source, MPC was used to optimize the torque distribution of motor and engine in receding horizon, which can effectively suppress the shift shock. For clutchless transmission, MPC avoids complex modeling and difficulty of online optimization control of clutch, showing better robustness and stability [25].

The PS-HEB equipped with a two-speed clutchless AMT is studied and segmented control method is applied in the gear shifting control strategy (GSCS) and adopts different control methods in different phases. The MPC-based coordinated control method is also used to compensate for torque variations in the powertrain, and the power source torque is coordinated and controlled to achieve a smooth shift process. In this study, the torque response model of the power system is reasonably simplified under the premise of satisfying the control accuracy, and the rolling optimization control in the shifting process is realized by quadratic programming (QP) [26]. Compared with the existing research, it has the characteristics of less computation and better real-time performance [27].

The remainder of the paper is organized as follows: Section 2 presents the vehicle architecture and the established models of the main components of the powertrain. In Section 3, the shifting control problems are analyzed. Section 4 presents the MPC-based GSCS and the QP solving method. Section 5 validates the GSCS by offline simulation. Section 6 concludes this study.

2 Powertrain Dynamic Modeling and Analysis

The research objects are a PS-HEB equipped with an SPGS (shown in Figure 1) and a two-speed clutchless AMT. The SPGS is used as power-split device, and the engine is connected to the planetary carrier while the motor/generator (MG) 1 is connected to the sun gear. The power of the SPGS is transmitted to the output shaft of the AMT by ring gear. The AMT is used to change the speed ratio of the drive motor (MG2) to the output shaft.

2.1 Engine Model

A single hidden layer back propagation neural network (BPNN) with 35 neurons is selected to establish the dynamic model of the engine in Ref. [28]. On flat and straight roads, the driver controls the pedal to allow the vehicle speed to frequently switch between high and low, thereby resulting in AMT frequent shift. The engine speed, torque, and throttle opening data during the shift are recorded as the training sample data of the engine neural network model. The expected output of the BPNN is engine torque, and the input of which includes engine speed and throttle opening data obtained from actual driving conditions.

Some other experimental data are collected to verify the generalization ability of engine model. The comparison between the torque output by the engine model and the actual engine torque is shown in Figure 2. Sudden change in torque is observed during engine start-up and shutdown phases. The torque output by the engine model has a slight deviation from the actual torque, but the output can follow actual torque in the remaining time. This finding shows that the BPNN model trained from engine running data can truly reflect the engine dynamic characteristics and has a good generalization ability.

2.2 Motor Model

In this section, the parameter identification principle of the least square method is adopted to identify the parameters of the first-order inertial model and finally obtain the dynamic motor model. The corresponding transfer function of the continuous system is as follows:

$$G_m(s) = \frac{T_{m,act}(s)}{T_{m,req}(s)} = \frac{K}{T \cdot s + 1}, \tag{1}$$

where $T_{m,req}$ and $T_{m,act}$ are the act torque and required torque of MG, K represents the scaling factor to be identified, and T is the response time constant of the motor to be identified. When $s \approx \frac{2}{T_s} \cdot \frac{1-Z^{-1}}{1+Z^{-1}}$ and T_s is the sampling time, Eq. (1) can be discretized by bilinear transformation as follows:

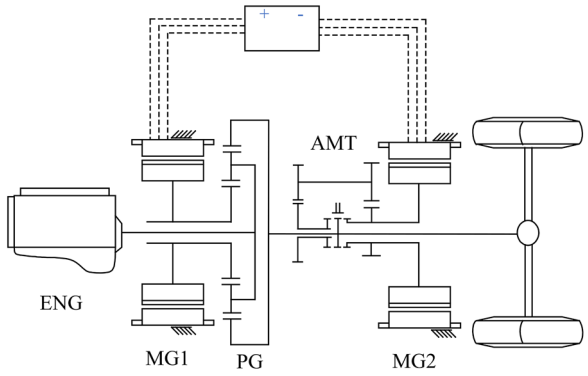

Figure 1 Structure of the PS-HEB powertrain

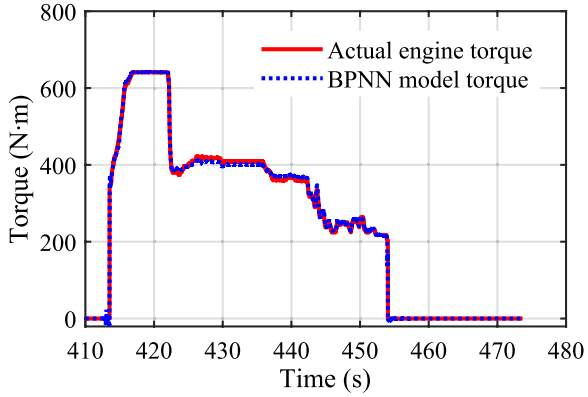

Figure 2 Torque response of BPNN engine model

$$T_{m,act}(t) = \alpha[T_{m,req}(t) + T_{m,req}(t-1)] - \beta T_{m,act}(t-1), \quad (2)$$

where $\alpha = K/(2T/T_s + 1), \beta = (1 - 2T/T_s)/(2T/T_s + 1)$.

In the running process, MG is affected by the rotary resistance moment, including bearing friction and ventilation resistance. Therefore, the transfer function of the motor is not strictly a first-order process, and an inevitable steady state error is found between $T_{m,req}$ and $T_{m,act}$. Compared with the actual output torque of the motor, the rotation resistance moment is small and generally not considered. An improved parameter identification method, which can identify the torque increase and torque decrease process and eliminate the adverse influence of rotation resistance moment on motor parameter identification as far as possible, is proposed to establish a more accurate motor transfer function model.

In accordance with the operating condition of the motor, the corresponding transfer function is selected, and the final fitting effect is shown in Figure 3. The figure shows that, in the selected working conditions, the first-order inertia model of the motor can better reflect the actual torque output characteristics.

2.3 Two-Speed AMT Model

The gear shifting actuator (GSA) uses direct current motor (DCM) as the power source, and ball screw or worm gear is used to convert the DCM torque into the flat power required for gear shifting. Thus, the gear shifting control accuracy is relatively high, and the cost is relatively low. The typical electric controlled AMT gearbox with high precision ball screw can achieve rapid and efficient shift. When the GSA receives the shift command, the DCM drives the screw and the connected shift fork to move in a straight line. When the speed of the input shaft synchronizes with the speed of the synchronizer, the transmission is shifted into the target gear. The mechanism model of the main components of the two-speed AMT gearbox is established in this section, including the gear shifting actuator, the synchronizer, the input, and output shaft of gearbox.

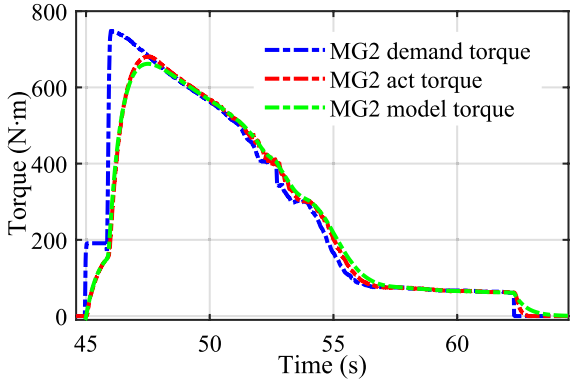

Figure 3 Dynamic model identification results of MG

2.3.1 GSA Model

The GSA comprises DCM and ball screw, and the DCM output shaft is fixedly connected with a ball screw nut. In the DCM, the torque balance relationship is as follows:

$$T_{s\_m} = I_{s\_m}\frac{\mathrm{d}\omega_{s\_m}}{\mathrm{d}t} + K_f\omega_{s\_m} + T_d, \quad (3)$$

where T_{s_m} is the output torque of DCM, I_{s_m} is the sum of the inertia of DCM and ball screw, K_f is the rotational damping coefficient of DCM, and T_d is the load torque of DCM.

The output torque of DCM is proportional to the motor current, as follows:

$$T_{s\_m} = K_m I, \quad (4)$$

where K_m is the motor torque constant.

In accordance with Eqs. (3) and (4), the DCM model is built in MATLAB/Simulink.

Then, the ball screw model is established. The driving torque on the screw is the load torque (T_d) on the DCM in Eq. (3). According to the principle of ball screw drive, the flat power generated by the driving torque on the nut is as follows:

$$F_l = \frac{2\pi}{h}T_d, \quad (5)$$

where h is the lead of the ball screw.

Considering the friction loss between the nut and the screw, on the premise of ignoring the damping force, the final output shifting force F_s of the screw nut is obtained as follows:

$$F_s = (1 - f)F_l. \quad (6)$$

In accordance with this relationship, the ball screw model was built, and the DCM and ball screw models were integrated to obtain the gear shift actuator model.

2.3.2 Synchronizer Model

The speed synchronization process of the synchronizer is an important link in the shifting process. In most articles, the contact reaction force generated between the locking ring and the gear ring during the synchronization stage is a constant value, and the resulting friction torque, namely, the synchronization torque, is a constant value [29, 30]. However, in fact, contact reaction force during synchronization is a complex process that gradually increases from 0 to shift force [31, 32]. To reduce the difficulty of modeling, the contact

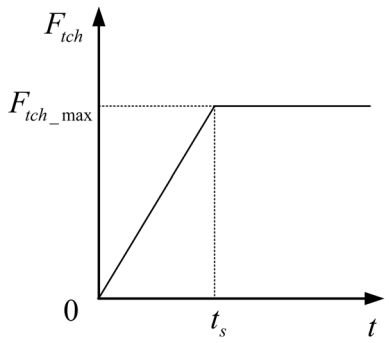

Figure 4 Variation trend of contact reaction force

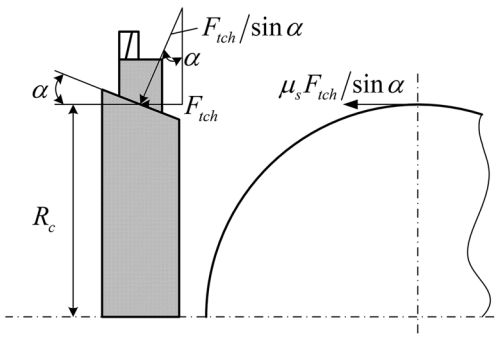

Figure 5 Dynamic model of synchronizer

reaction force at the synchronization stage is assumed to increase linearly with time from 0, reach the maximum value after time t_s, and remain stable, as shown in Figure 4.

The kinetic model of the synchronizer in the synchronization stage is established, as shown in Figure 5.

When the contact reaction force of the synchronizer is F_{tch}, the synchronization torque of the locking ring acting on the gear ring is as follows:

$$T_{syn1} = \frac{\mu_s F_{tch} R_c}{\sin\alpha}, \tag{7}$$

where T_{syn1} is the synchronizing torque acting on the gear ring of AMT, μ_s is the friction coefficient of cone surface, R_c is the average effective radius of friction of the cone, and α is the half cone angle.

2.3.3 Input Shaft Model

The main function of the AMT input shaft model is to calculate the motion state of the input shaft according to the internal dynamics and kinematics of AMT. When the synchronizer and gear ring are completely engaged, the speed of the MG2 input shaft is obtained as follows:

$$n_{a\_in} = \omega_r i_g, \tag{8}$$

where n_{a_in} is the speed of the input shaft, ω_r is the speed of carrier, and i_g is the ratio of AMT.

Assuming that the input shaft speed remains unchanged during the process of synchronizer separation and re-engagement, and the input shaft speed in the process of re-engagement is as follows:

$$n_{a\_in} = n_0 + \int_0^{t_d} (T_{syn1}/i_g + T_m)/(I_m + I_a)\mathrm{d}t, \tag{9}$$

where n_0 represents the speed of input shaft before shifting, and t_d is the duration of gear shifting process, T_m is MG2 torque, I_a represents the moment of inertia of the AMT equivalent to the input shaft, which can be expressed as =:

$$I_a = I_1 + \frac{I_2}{i_{12}} + \frac{I_3}{i_{12} i_{23}}, \tag{10}$$

where I_a is the equivalent moment of inertia of the AMT; I_1, I_2, and I_3 are moment of inertia of input shaft, intermediate shaft, and output shaft, respectively; i_{12} is the ratio of input shaft to intermediate shaft; i_{23} is the ratio of intermediate shaft to output shaft.

When the gearbox shifts from low-speed gear to high, the speed of the high gear on the output shaft is higher than that of the synchronizer. The synchronous torque hinders the rotation of MG2 and the input shaft of the gearbox during the synchronization process. On the contrary, during downshifts, the synchronous torque accelerates the rotation of MG2 and gearbox input shaft.

2.3.4 Output Shaft Model

The gearbox output shaft model focuses on the external output characteristics of the AMT and is used to calculate the output torque. When not shifting, the MG2 torque is the output torque of the gearbox after overcoming the torque consumed by MG2 inertia and gearbox inertia. In the shifting process, the output torque of AMT is T_{syns2}, the synchronous torque acting on the output shaft, the same magnitude, and opposite direction with T_{syns1}.

When not shifting, the torque of the AMT output shaft is calculated using Eq. (11).

$$T_{a\_out} = i_g(T_m - (I_m + I_a)\dot{\omega}_m), \tag{11}$$

where, $\dot{\omega}_m$ denotes the angular acceleration of MG2.

When shifting, the torque of the AMT output shaft is calculated as Eq. (12).

$$T_{a\_out} = i_g(T_m - (I_m + I_a)\dot{\omega}_m) + T_{syn2}. \tag{12}$$

2.3.5 Model Integration and Validation

The AMT model is obtained by integrating the models mentioned above, and the accuracy of the model is further verified by simulation. With the driver's pedals as input, partial signals of the vehicle and transmission during acceleration are obtained, as shown in Figure 6.

The test results show that the synchronizing torque acting on MG2 is 0 prior to shifting. The AMT begins to shift from low-speed gear to high-speed gear at 20 s. At this time, the MG2 torque changes to 0, the synchronizing torque acting on the input shaft increases in reverse, and the speed of MG2 declines. Meanwhile, the synchronizing torque has a driving effect on the vehicle, and the output torque of AMT increases gradually with the synchronizing torque. When the MG2 speed declines to the target speed, the synchronizing torque disappears, and the input shaft engages with the output shaft to complete the shift. At 25 s, the gearbox starts to shift from high-speed gear to low-speed gear, and the synchronizing torque increases positively. The synchronizing torque acting on input shaft is smaller than that of the up-shift process due to the larger transmission ratio. Thus, the MG2 speed synchronization time is increased. The synchronizing torque is the resistance torque for the driving wheel during the process, the gearbox outputs the negative torque until the end of the upshift process. The change in system output torque has insignificant impact on the vehicle speed due to the short duration of gear shifting.

The simulation results show that the AMT model can reflect the internal dynamic relationship and external output characteristics of the transmission. Thus, the expected design goal is achieved, and the requirements of simulation accuracy of the entire powertrain are satisfied.

2.4 Longitudinal Dynamics Model

Ignoring the rotational viscous damping, elastic deformation of bearing, and meshing deformation of gear, the basic dynamic relations of SPGS are shown in Eqs. (13)–(15).

$$I_r\dot{\omega}_r = F \cdot R - T_r, \tag{13}$$

$$(I_e + I_c)\dot{\omega}_e = T_e - F \cdot R - F \cdot S, \tag{14}$$

$$(I_g + I_s)\dot{\omega}_g = F \cdot S - T_g, \tag{15}$$

where T_r, T_e, and T_g denote the ring torque, engine torque, and MG1 torque, respectively; I_r, I_c, and I_s represent the moment of inertia of ring gear, planetary carrier, and sun gear, respectively; I_e and I_g are moment of inertia of engine and MG1, respectively; ω_r, ω_e, and ω_g are speed of ring gear, engine, and MG1, respectively; R and S are the radii of the ring gear and sun gear, respectively; F is the internal force of SPGS.

The characteristic parameter (the ratio of ring gear teeth to sun gear teeth) of SPGS is defined as k_p, as follows:

$$k_p = \frac{R}{S}. \tag{16}$$

According to Eqs. (13), (14), and (16), T_r can be expressed as follows:

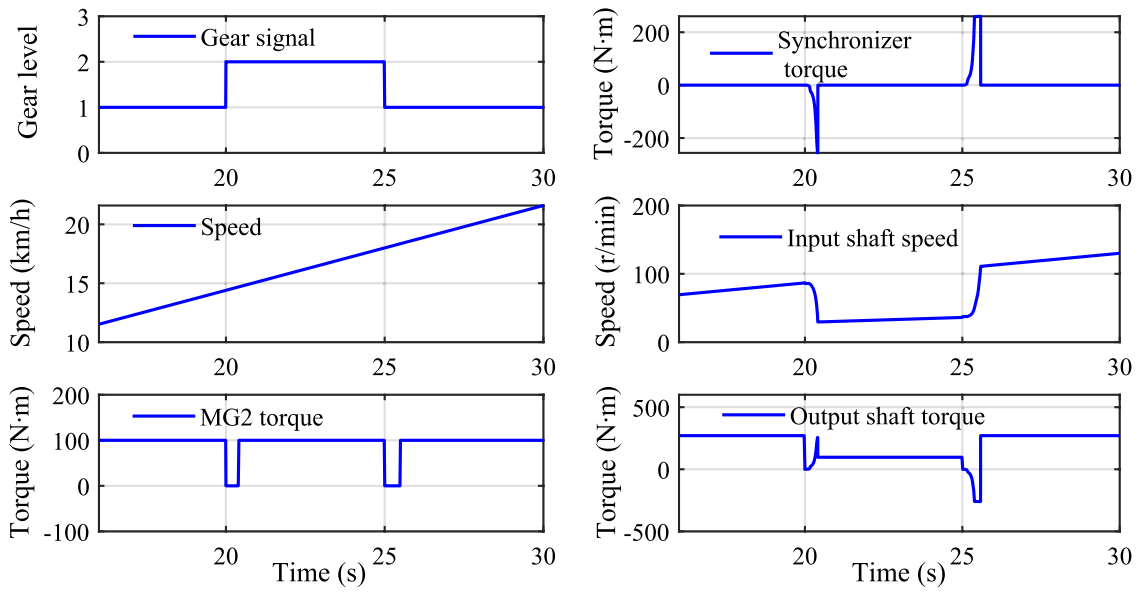

Figure 6 Simulation results of the shifting process of two-speed AMT

$$T_r=\frac{k_p}{1+k_p}T_e-I_r\dot{\omega}_r-\frac{k_p}{1+k_p}(I_e+I_c)\dot{\omega}_e. \tag{17}$$

Then, according to the AMT model, the AMT dynamic equation can be obtained using Eq. (18), as follows:

$$i_g^2(I_m+I_a)\dot{\omega}_r=T_m i_g+T_{syn2}-T_a. \tag{18}$$

The output torques of ring gear and AMT are coupled to the drive wheel to overcome vehicle driving resistance. If only longitudinal dynamics of the vehicle is considered, then the following relationship can be obtained:

$$\left(\frac{n_tI_t}{R_t}+MR_t\right)\frac{\dot{\omega}_rR_t}{i_0}=(T_r+T_a)i_0-T_f, \tag{19}$$

where T_f is the driving resistance of the bus, I_t is the wheel inertia, n_t is the number of wheel, M is the vehicle mass, a is longitudinal acceleration, R_t is the wheel radius, and i_0 is the final drive ratio.

On the basis of this analysis, the longitudinal dynamic equation between SPGS and driving wheels can be obtained by combining Eqs. (17), (18), and (19), as follows:

$$\begin{aligned}&\left(\frac{k_p}{1+k_p}T_e+T_mi_g+T_{syn}\right)i_0-T_f\\&=\frac{k_p}{1+k_p}(I_e+I_c)\dot{\omega}_ei_0+\left[i_g^2i_0^2(I_m+I_a)+I_ri_0^2+n_tI_t+MR_t^2\right]\frac{\dot{\omega}_r}{i_0}.\end{aligned} \tag{20}$$

3 Analysis of Shifting Control Problems

The relationship between the speed v of bus and the speed ω_r of ring gear is combined, and the expression jerk of the bus is as follows:

$$j=\frac{\mathrm{d}a}{\mathrm{d}t}=\frac{\ddot{\omega}_r}{R_t}i_0. \tag{21}$$

On the basis of Eqs. (17) and (20), the longitudinal jerk can be described by the difference of the ring gear angular acceleration, as follows:

$$\begin{aligned}&\ddot{\omega}_r\left[\frac{I_v'}{k_p^2i_oI_g'}+\frac{(1+1/k_p)^2I_v'}{i_oI_e}+1\right]\\&=-\frac{1}{k_pI_g'}\dot{T}_g+\left[\frac{(1+1/k_p)^2}{I_e}+\frac{1}{k_p^2I_g'}\right]\dot{T}_{a\_out}\\&+\frac{1+1/k_p}{I_e}\dot{T}_e-\left[\frac{(1+1/k_p)^2}{i_oI_e}+\frac{1}{k_p^2i_oI_g'}\right]\dot{T}_f,\end{aligned} \tag{22}$$

where $I_v'=i_g^2i_o(I_m+I_a)+I_ri_o+n_tI_t/i_0+MR_t^2/i_o$, $I_g'=I_s+I_g, I_g'=I_s+I_g$.

Equation (22) shows that the coefficient of $\ddot{\omega}_r$ is a constant. Thus, $\ddot{\omega}_r$ is only determined by the four terms at the right side of Eq. (22). The vehicle is a large-inertia system; thus, the shifting process is short, which does not cause sudden change in vehicle speed, nor will the driving resistance relate to the vehicle speed. Therefore, the term $\left[\frac{(1+1/k_p)^2}{i_oI_e}+\frac{1}{k_p^2i_oI_g'}\right]\dot{T}_f$ is small and can be ignored, and the system jerk mainly depends on the torque of engine, MG1, and output shaft of AMT. The output torque of AMT depends on MG2 and synchronizer. The control objects are engine, MG1, and MG2 because the synchronizing torque is controlled by the transmission control unit (TCU).

When the bus is running, the gear changes with the demand torque and speed. The gear shifting process is divided into five phases, including (I) unload of MG2, (II) shift to neutral gear, (III) active speed synchronization by MG2, (IV) engage to new gear, and (V) resuming the power. Taking hybrid drive mode as an example, the entire shifting process is symbolically illustrated.

The control in phase I aimed at reducing the torque of MG2 to zero and preparing for AMT to shift to neutral gear. In this phase, a coordinated control strategy based on MPC was developed to reduce the jerk of the vehicle during MG2 unloading. When the torque of MG2 drops to 0, the actuator acts and shifts to neutral gear. In phase III, the AMT remains in neutral gear, and the connection of MG2 and driving system is cut off. By controlling MG2, the speed of the target gear ring and lock ring of the synchronizer are synchronized to reduce the shift time and extend the service life of the synchronizer. When the speed of the gear ring is close to the lock ring of the synchronizer, the AMT switches to phase IV, the actuator drives the sliding sleeve to move, and then shifts to new gear. After shifting, in phase V, the MG2 resumes torque output.

The upshift process in the hybrid mode is considered an example to study the proposed GSCS due to the same control method of upshift and downshift. In phases II and IV, the vehicle control unit (VCU) only needs to send corresponding actuating signals to TCU, and TCU control the GSA to achieve relevant operations. For phase III, MG2 can be switched to speed control mode to actively realize speed synchronization because it is unconnected to the power system and has no impact on the system jerk. Therefore, the control problem of phases I and V is mainly studied. When the MG2 torque decreases in phase I or increases in phase V, engine and MG1 shall rapidly compensate for the MG2 torque changes.

4 MPC-Based Coordinated Control of Phases I and V

In this section, on the basis of the characteristics of power system components in Section 2, the prediction model of powertrain is established. Then, the optimal MG1 torque sequence is obtained by the QP method in

phases I and V, and the coordinated control of each component is realized on the basis of MPC.

4.1 Prediction Model of Powertrain

In phases I and V, the synchronous torque is 0. According to the longitudinal dynamic model, the state equation of SPGS to driving wheel can be obtained, as follows:

$$\frac{k_p}{1+k_p}(I_e+I_c)\dot{\omega}_e i_0 = \frac{k_p i_0}{1+k_p}T_e + T_m i_g i_0 - \delta MaR_t - T_f, \tag{23}$$

where $\delta Ma = \left[i_g^2 i_0^2(I_m+I_a) + I_r i_0^2 + n_t I_t + MR_t^2\right]\dot{\omega}_r/i_0$, MR_t^2 is the inertia moment of the vehicle mass equivalent to wheels, $\left[i_g^2 i_0^2(I_m+I_a) + I_r i_0^2 + n_t I_t\right]$ is the inertia moment of the transmission system equivalent to wheels, and δ is the rotation mass conversion factor.

Considering the engine speed as the state variable, the engine torque as the control variable, and the MG2 torque and the vehicle driving resistance moment as the disturbance variables, the system state space equation is established, as shown in Eq. (24).

$$\begin{cases} \dot{x} = A_c x + B_{cu} u + B_{cd} d, \\ y = C_c x, \end{cases} \tag{24}$$

where $x = \omega_e$, $u = T_e$, $d = T_m i_g i_o - \delta MaR_t - T_f$, $A_c = 0$, $B_{cu} = (I_c + I_e)^{-1}$, $C_c = 1$, $B_{cd} = \left[\frac{k_p i_0}{1+k_p}(I_c+I_e)\right]^{-1}$.

The discrete model can be derived by precise discretization method, as shown in Eq. (25).

$$\begin{cases} x(k+1) = Ax(k) + B_u u(k) + B_d d(k), \\ y_c(k) = C_c x(k), \end{cases} \tag{25}$$

where $A = e^{A_c T_s} = I$, $B_u = \int_0^{T_s} e^{A_c t}\mathrm{d}t \cdot B_{cu} = B_{cu} T_s$, $B_d = \int_0^{T_s} e^{A_c t}\mathrm{d}t \cdot B_{cd} = B_{cd} T_s$.

Incremental control is adopted to reduce the steady-state error. The incremental model is obtained based on Eq. (26):

$$\begin{cases} \Delta x(k+1) = A\Delta x(k) + B_u \Delta u(k) + B_d \Delta d(k), \\ y_c(k) = C_c \Delta x(k) + y_c(k-1), \end{cases} \tag{26}$$

where $\Delta x(k) = x(k) - x(k-1)$, $\Delta u(k) = u(k) - u(k-1)$, $\Delta d(k) = d(k) - d(k-1)$.

According to the control principle of MPC, the predictive horizon and control horizon are defined as m and p, respectively, thereby confirming that $m \geq p$. In addition, the following assumptions are made: ① Outside the control domain, the control quantity remains unchanged, $\Delta u(k+i) = 0$, $(i = m, m+1, \ldots)$; ② δMaR_t and T_f of the disturbance quantity Δd remain unchanged in the prediction time domain, $\Delta d(k+i) = T_m i_g i_0$, $(i = m, m+1, \ldots)$.

For assumption ①, the prediction of future system states requires control variables of the entire predictive horizon when the control horizon is smaller than the predictive horizon. For assumption ②, because the duration of the shift process is short, the speed change is small, and the driving resistance is unchanged significantly. Thus, the disturbance of the system state space equation is only MG2 torque.

With this assumption, the system output in the predictive horizon is defined as follows:

$$\boldsymbol{Y}_c(k+1|k) = \begin{bmatrix} y_c(k+1|k) \\ y_c(k+2|k) \\ \vdots \\ y_c(k+p|k) \end{bmatrix}, \tag{27}$$

where $y_c(k+p|k)$ represents the prediction of time $k+p$ at time k.

The control sequence of the system in the control horizon is as follows:

$$\Delta\boldsymbol{U}(k) = \begin{bmatrix} \Delta u(k) \\ \Delta u(k+1) \\ \vdots \\ \Delta u(k+m-1) \end{bmatrix}. \tag{28}$$

Then, the prediction equation of the system, which is the relationship between system output and system input in the prediction horizon, can be derived as follows:

$$\boldsymbol{Y}_c(k+1|k) = \boldsymbol{S}_x \Delta x(k) + \boldsymbol{I}_c y_c(k) + \boldsymbol{S}_d \Delta d(k) + \boldsymbol{S}_u \Delta\boldsymbol{U}(k), \tag{29}$$

where $\boldsymbol{S}_x$, $\boldsymbol{I}_c$, $\boldsymbol{S}_d$, and $\boldsymbol{S}_u$ are expressed as follows:

$$\boldsymbol{S}_x = \begin{bmatrix} C_c A & \sum_{i=1}^{2} C_c A^i & \cdots & \sum_{i=1}^{N_p} C_c A^i \end{bmatrix}^{\mathrm{T}}, \tag{30}$$

$$\boldsymbol{I}_c = \begin{bmatrix} 1 & 1 & \cdots & 1 \end{bmatrix}^{\mathrm{T}}, \tag{31}$$

$$\boldsymbol{S}_d = \begin{bmatrix} C_c B_d & C_c A B_d + C_c B_d & \cdots & \sum_{i=1}^{N_p} C_c A^{i-1} B_d \end{bmatrix}^{\mathrm{T}}, \tag{32}$$

$$\boldsymbol{S}_u = \begin{bmatrix} C_cB_u & 0 & \cdots & 0 \\ \sum_{i=1}^{2} C_cA^{i-1}B_u & C_cB_u & \cdots & 0 \\ \vdots & \vdots & \ddots & \vdots \\ \sum_{i=1}^{m} C_cA^{i-1}B_u & \sum_{i=1}^{m-1} C_cA^{i-1}B_u & \cdots & C_cB_u \\ \vdots & \vdots & \ddots & \vdots \\ \sum_{i=1}^{p} C_cA^{i-1}B_u & \sum_{i=1}^{p-1} C_cA^{i-1}B_u & \cdots & \sum_{i=1}^{p-m+1} C_cA^{i-1}B_u \end{bmatrix}. \tag{33}$$

4.2 QP-based Optimal Control

Engine speed and torque are considered control targets to ensure that SPGS compensates for the change in MG2 torque, and the influence of abrupt change of engine speed on system stability is avoided. The control targets of engine speed and MG1 torque are described as follows:

$$\boldsymbol{R}_1(k+1) = \left[\omega_{e\_tar}(k+1), \omega_{e\_tar}(k+2), \ldots, \omega_{e\_tar}(k+i), \ldots, \omega_{e\_tar}(k+p)\right]^{\mathrm{T}}, \tag{34}$$

$$\boldsymbol{R}_2(k+1) = \left[T_{e\_tar}(k+1), T_{e\_tar}(k+2), \ldots, T_{e\_tar}(k+i), \ldots, T_{e\_tar}(k+p)\right]^{\mathrm{T}}, \tag{35}$$

where ω_{e_tar} is the target engine speed sequence during phase I.

The engine speed prior to phase I was considered the target speed of the engine, that is, $R_e(k+1) = I_c\omega_e(k)$ due to the short duration of phase I; $T_{g\_tar}(k+i)$ is the MG1 target torque at time $k+i$, which can be obtained by combining Eqs. (17) and (18):

$$T_{e\_tar}(k+i) = T_{dr}\frac{1+k_p}{k_p} + (I_e + I_c)\dot{\omega}_e - T_m i_g \frac{1+k_p}{k_p}, \tag{36}$$

where $T_{dr}(k)$ is the driving torque required by the driver for the output shaft of the powertrain at time k. The target driving torque is also assumed to be the same in the control horizon because the shift time is very short, and the target torque of MG1 is linearly dependent on the torque of MG2.

Considering the system requirements during phases I and V, the optimization objective is formed as follows:

$$\min_{\Delta U(k)} J(x(k), \Delta\boldsymbol{U}(k), m, p), \tag{37}$$

where Q_1 and Q_2 are the weight factors for adjusting tracking performance. This optimization problem in Eq. (38) is constrained and transformed into a QP problem. As shown in Eq. (38), QP solution is conducted to obtain the optimal torque sequence of the engine.

The system constraints mainly consist of the peak value limitation and the variation rate limitation. First, the maximum and minimum values of T_e are limited by the external characteristics of the engine. Second, in accordance with these assumptions, the ring gear speed is assumed to maintain in the prediction horizon. T_g should be further limited according to the battery power limitation to ensure the driving performance and to protect the battery. Combined with these considerations, the peak torque of MG1 is limited as follows:

$$\begin{cases} T_{g\min}(k+i) \le T_g(k+i) \le T_{g\max}(k+i), \\ i = 0, 1, \ldots, m-1, \end{cases} \tag{39}$$

where $T_{g\min}$ and $T_{g\max}$ are the lower and upper limits of MG1 torque.

In accordance with the upper and lower limits of engine torque ($T_{e\max}$ and $T_{e\min}$), engine torque constraint can be obtained as follows:

$$\begin{cases} T_{e\min}(k+i) \le T_e(k+i) \le T_{e\max}(k+i), \\ i = 0, 1, \ldots, m-1. \end{cases} \tag{40}$$

The minimum engine torque $T_{e\min} = 0$ and the maximum engine torque is calculated as:

$$T_{e\max} = \min\left\{T_{e\_ec}, (1+k_p)T_{g\_ec}\right\}, \tag{41}$$

where T_{e_ec} and T_{g_ec} are the full-load torque of engine and MG1.

On the basis of the established dynamic model of the engine, the maximum and minimum values of engine torque increment ΔT_e within sampling time T_s are tested when engine load increases from 0 step to 100% and decreases from 100% step to 0 at different speeds to limit engine torque change ΔT_e. The constraints are as follows:

$$J = \left\|Q_1 \cdot (\boldsymbol{Y}_c(k+1|k) - \boldsymbol{R}_1(k+1))\right\|^2 + \left\|Q_2 \cdot (\Delta\boldsymbol{U}(k) - \boldsymbol{R}_2(k+1))\right\|^2, \tag{38}$$

$$\begin{cases} \Delta T_{e\min}(k+i) \le \Delta T_e(k+i) \le \Delta T_{e\max}(k+i), \\ i = 0, 1, \ldots, m-1. \end{cases} \tag{42}$$

In addition, to prevent the engine speed from exceeding the limit during phase I, the engine idle speed and the maximum engine speed are considered the upper and lower limits of the engine speed range in the optimization process, respectively, as follows:

$$\begin{cases} \omega_{e\min}(k+i) \le \omega_e(k+i) \le \omega_{e\max}(k+i), \\ i = 1, 2, \ldots, p. \end{cases} \tag{43}$$

Considering all the constraints, the QP optimization problem described by Eqs. (37) and (38) can be rewritten as follows:

$$\begin{aligned} &\min_{\Delta U(k)} \frac{1}{2}\Delta \boldsymbol{U}(k)^{\mathrm{T}} H \Delta \boldsymbol{U}(k) + \boldsymbol{G}(k+1|k)^{\mathrm{T}} \Delta \boldsymbol{U}(k), \\ &\text{s.t.,} \quad C_u \Delta \boldsymbol{U}(k) \le b(k+1|k), \end{aligned} \tag{44}$$

where

$$\boldsymbol{H} = 2(\boldsymbol{S}_u^{\mathrm{T}} \boldsymbol{Q}_1^{\mathrm{T}} Q_1 S_u + \boldsymbol{Q}_2^{\mathrm{T}} Q_2), \tag{45}$$

where

$$\boldsymbol{Y}_{\min}(k+1) = \begin{bmatrix} \omega_{e\min}(k+1) \\ \omega_{e\min}(k+2) \\ \vdots \\ \omega_{e\min}(k+p) \end{bmatrix}, \tag{49}$$

$$\boldsymbol{Y}_{\max}(k+1) = \begin{bmatrix} \omega_{e\max}(k+1) \\ \omega_{e\max}(k+2) \\ \vdots \\ \omega_{e\max}(k+p) \end{bmatrix}. \tag{50}$$

On the basis of the QP theory, the optimum engine torque control sequence can be derived, and the first value of $\Delta \boldsymbol{U}(k)$ is selected as the engine torque increment command at time k. The optimal torque changes with the rolling update of the system state until the end of phase I or V.

Assuming that the optimal act torque of the engine at time k is $T_{e\_act}(k)$, the target torque of MG1 can be obtained according to Eqs. (14) and (15):

$$\begin{aligned} \boldsymbol{G}(k+1|k) = {} & 2\boldsymbol{S}_u^{\mathrm{T}} \boldsymbol{Q}_1^{\mathrm{T}} Q_1 \left(\boldsymbol{S}_x \Delta x(k) + I_c y_c(k) + \boldsymbol{S}_d \Delta d(k) - \boldsymbol{R}_1(k+1) \right) \\ & - 2\boldsymbol{Q}_2^{\mathrm{T}} Q_2 \boldsymbol{R}_2(k+1), \end{aligned} \tag{46}$$

$$\boldsymbol{C}_u = \begin{bmatrix} \boldsymbol{I} & -\boldsymbol{I} & \boldsymbol{L}^{\mathrm{T}} & -\boldsymbol{L}^{\mathrm{T}} & \boldsymbol{S}_u^{\mathrm{T}} & -\boldsymbol{S}_u^{\mathrm{T}} \end{bmatrix}^{\mathrm{T}}, \tag{47}$$

where, I is a unit matrix, and L is a lower triangular matrix in which all the elements are unit matrix.

$$\boldsymbol{b}(k+1|k) = \begin{bmatrix} \Delta T_{e\max}(k) \\ \vdots \\ \Delta T_{e\max}(k+m-1) \\ -\Delta T_{e\min}(k) \\ \vdots \\ -\Delta T_{e\min}(k+m-1) \\ T_{e\max}(k) - u(k-1) \\ \vdots \\ T_{e\max}(k+m-1) - u(k-1) \\ u(k-1) - T_{e\min}(k) \\ \vdots \\ u(k-1) - T_{e\min}(k+m-1) \\ \boldsymbol{Y}_{\max}(k+1) - \boldsymbol{I}Y(k) - S_x \Delta x(k) - S_x \Delta d(k) \\ -\boldsymbol{Y}_{\min}(k+1) + \boldsymbol{I}Y(k) + S_x \Delta x(k) + S_x \Delta d(k) \end{bmatrix}, \tag{48}$$

$$\begin{aligned} T_g(k) = {} & \left[\frac{I_e + I_c}{1+k_p} + (1+k_p)(I_g + I_s) \right] \dot{\omega}_e(k) \\ & - \frac{T_{e\_act}(k)}{1+k_p} - k_p(I_g + I_s)\dot{\omega}_r(k). \end{aligned} \tag{51}$$

5 Simulation and Analysis

To validate the control effect of the proposed MPC-based GSCS, a PID-based GSCS fully and accurately is designed. These strategies are combined with vehicle energy management strategy to carry out offline simulation, and the simulation results are analyzed. The vehicle simulation model consists of driving cycle, driver model, vehicle model, and control strategy, which is a forward simulation model. The driver model follows the target speed by controlling the accelerator pedal and brake pedal. For the PID-based GSCS, the target torque of the engine is directly calculated according to Eq. (8). MG1 adopts PID control method, with the engine speed before shifting as the control target, and the torque of MG1 is adjusted to ensure that the engine speed is stable. The MG1 torque is calculated as:

$$\begin{cases} T_g(k) = K_p \cdot e(k) + K_i \sum_{i=0}^{k} e(i) + K_d[e(k) - e(k-1)], \\ e(k) = \omega_{e,tar} - \omega_e(k), \end{cases} \tag{52}$$

where, K_p, K_i, and K_d denote the proportionality coefficient, integration coefficient and difference coefficient respectively, and e is the deviation between the actual and target engine speed.

The principle of upshift and downshift is the same, and only the state changes of the powertrain in the upshift process are listed. The simulation results of the two GSCSs are compared, as shown in Figures 7, 8, 9, which are the speed and torque of power sources and the entire powertrain during acceleration. Figure 7 shows that in the phase I of the shifting process, the engine torque increases with the decrease in MG2 torque to compensate for the change in the MG2 torque. Correspondingly, in phase V, the engine torque decreases with the increase in MG2 torque. In phases II, III, and IV, AMT has no torque output, and the engine torque changes with the driving demand torque. Compared with the MPC-based GSCS, torque changes of the engine and MG1 under PID-based GSCS have significant lag, and the MG1 torque has a significant oscillation in the early stages of phases I and V. Figure 8 shows that under the PID method, the engine speed increases by 104 r/min within 1 s. However, the engine speed is stable under the MPC-based GSCS. The torque of the two GSCS approaches remained consistent because they adopted the same control method for the MG2. In phase IV, MG2 adopts larger torque to achieve the target speed as soon as possible. For the entire powertrain, as shown in Figure 9, when the MPC-based GSCS

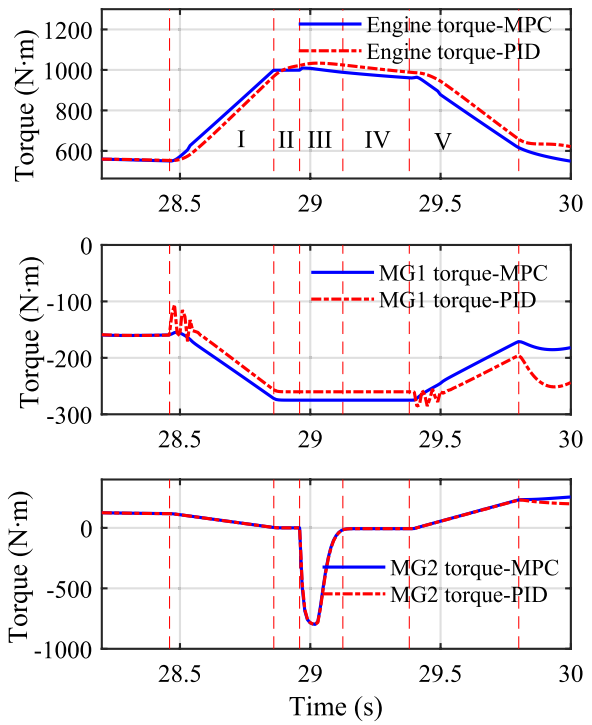

Figure 7 Torque of power sources when shifting

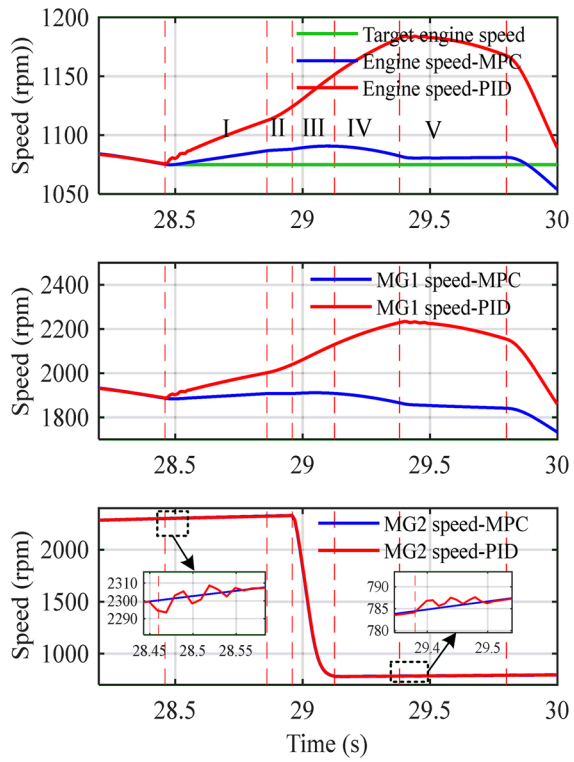

Figure 8 Speed of power sources when shifting

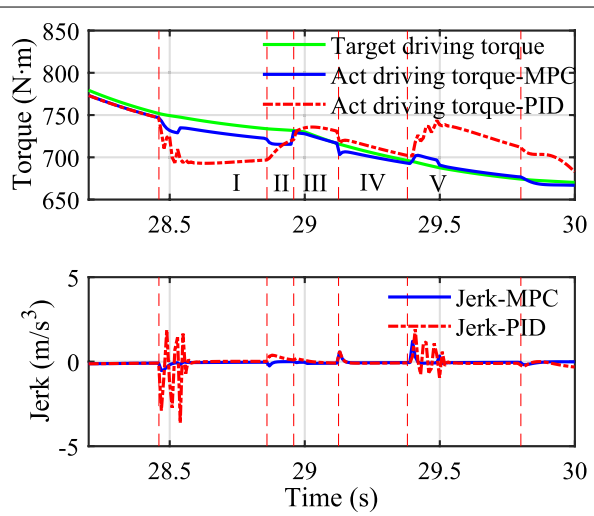

Figure 9 Driving torque and system jerk

is adopted, the torque of the powertrain changes gently and closer to the driving demand torque. In addition, the maximum jerk of the system is up to 1.2 m/s^3. When the PID-based GSCS is adopted, the driving torque deviates significantly from the driving demand torque and fluctuates violently. The maximum jerk of the system is up to 3.6 m/s^3. Compared with PID-based method, the MPC-based GSCS can not only ensure the stable torque output of power system, but also the stability of engine speed, which is significantly better than PID method. Therefore, the proposed GSCS can effectively reduce the shift jerk and improve the driving comfort.

6 Conclusions

The characteristics of powertrain are studied, and an MPC-based GSCS, which can effectively suppress the shift jerk and ensure the stability of the powertrain in the shifting process, is proposed, considering the SPGS hybrid power system with a clutchless two-speed AMT as the research object. The main contributions of this study are as follows.

(1) The dynamic model of the powertrain is established by combining the methods of data-driven modeling and mechanism modeling, considering the accuracy and simulation efficiency. On the basis of the parameter identification method, the first-order inertia models of the motors are established, thereby combining the increasing and decreasing torque conditions. In addition, the two-speed clutchless AMT gearbox mechanism model is established on the basis of the analysis of the working mechanism.

(2) A segmented control method combining MPC for GSCS is proposed. The MPC-based dynamic coordination control strategy is established in the key phases I and V (i.e., the phases when the output torque of MG2 gradually decreases and increases), and the QP is used to realize the optimal control of the engine and MG1. Thus, the powertrain torque and engine speed become stable during the gear shift. The simulation results verify the effectiveness of the proposed GSCS. Compared with the commonly used PID control strategy, the proposed MPC-based GSCS has significant advantages.

Acknowledgements
Not applicable.

Author Contributions
XZ was in charge of the whole trial; TL wrote the manuscript; DS assisted with sampling and laboratory analyses. All authors read and approved the final manuscript.

Authors' Information
Tong Liu is currently pursuing the Ph.D. degree at *College of Automotive Engineering, Changchun Jilin University, China.*
Xiaohua Zeng is currently a professor at *State Key Laboratory of Automotive Simulation and Control, Jilin University, Changchun, China*. He received his Ph.D. degree in vehicle engineering from *Jilin University, China,* in 2006.
Dafeng Song is currently a professor at *State Key Laboratory of Automotive Simulation and Control, Jilin University, China* and she received her Ph.D. degree in vehicle engineering from *Jilin University, China*, in 2005.

Funding
Supported by National Natural Science Foundation of China (Grant No. 52272394).

Competing Interests
The authors declare no competing financial interests.

Received: 4 November 2021 Revised: 12 July 2022 Accepted: 8 November 2022
Published online: 03 December 2022

References

[1] Y L Yang, H X Pei, X S Hu, et al. Fuel economy optimization of power split hybrid vehicles: A rapid dynamic programming approach. *Energy*, 2019, 166: 929-938.
[2] W R Geng, D M Lou, C Wang, et al. A cascaded energy management optimization method of multimode power-split hybrid electric vehicles. *Energy*, 2020, 199: 117224.
[3] B Zhang, J Y Zhang, F G Xu, et al. Optimal control of power-split hybrid electric powertrains with minimization of energy consumption. *Applied Energy*, 2020, 266: 114873.
[4] X Y Lin, Y L Li, B Xia. An online driver behavior adaptive shift strategy for two-speed AMT electric vehicle based on dynamic corrected factor. *Sustainable Energy Technologies and Assessments*, 2021, 48: 101598.
[5] J Cui, G Tan, Z Tian, et al. Parameter optimization of two-speed AMT electric vehicle transmission system. SAE, 2020, 2020-01-0435.
[6] L Glielmo, L Iannelli, V Vacca, et al. Gearshift control for automated manual transmissions. *IEEE/ASME Transactions on Mechatronics*, 2006, 11(1): 17-26.
[7] H S Jo, Y I Park, J M Lee, et al. A development of an advanced shift control algorithm for a hybrid vehicles with automated manual transmission. *International Journal of Heavy Vehicle Systems*, 2000, 7(4): 281-298.
[8] S B Xie, X S Hu, K Lang, et al. Powering mode-integrated energy management strategy for a plug-in hybrid electric truck with an automatic mechanical transmission based on pontryagin's minimum principle. *Sustainability*, 2018, 10(10): 3758.
[9] J Q Li, H Wei, F C Sun, et al. Coordinated control of downshift powertrain of combined clutch transmissions for electric vehicles. *Energy Procedia*, 2014, 61: 1917-1920.
[10] G Xia, J S Chen, X W Tang, et al. Shift quality optimization control of power shift transmission based on particle swarm optimization–genetic algorithm. *Proceedings of the Institution of Mechanical Engineers, Part D: Journal of Automobile Engineering*, 2022, 236(5): 872-892.
[11] C L Liao, J Z Zhang, Q C Lu. Coordinated powertrain control method for shifting process of automated mechanical transmission in the hybrid electric vehicle. *Journal of Mechanical Engineering*, 2005, 41(12): 37-41.
[12] M Pettersson, L Nielsen. Gear shifting by engine control. *IEEE Transactions on Control Systems Technology*, 2000, 8(3): 495-507.
[13] Z Zhong, G Kong, Z Yu, et al. Shifting control of an automated mechanical transmission without using the clutch. *International Journal of Automotive Technology,* 2012, 13(3): 487-496.
[14] J T Fu, S Z Song, Z M Fu, et al. Design of coordinated control strategy during driving mode switching for parallel hybrid electric vehicles. *Transactions of the Institute of Measurement and Control*, 2019, 41(9): 2507-2520.
[15] S B Xie, X S Hu, Z K Xin, et al. Pontryagin's minimum principle based model predictive control of energy management for a plug-in hybrid electric bus. *Applied energy,* 2019, 236: 893-905.

[16] X H Zeng, X M Zhang, D P Yang, et al. Dynamic coordination control for hydraulic hub-motor auxiliary system based on NMPC algorithm. *Measurement*, 2022, 191: 110795.
[17] X H Zeng, N N Yang, J X Wang, et al. Predictive-model-based dynamic coordination control strategy for power-split hybrid electric bus. *Mechanical Systems and Signal Processing*, 2015, 60: 785-798.
[18] Y Z Su, M H Hu, J Huang, et al. Dynamic torque coordinated control considering engine starting conditions for a power-split plug-in hybrid electric vehicle. *Applied Sciences*, 2021, 11(5): 2085.
[19] Y L Qi, C L Xiang, W D Wang, et al. Model predictive coordinated control for dual-mode power-split hybrid electric vehicle. *International Journal of Automotive Technology*, 2018, 19(2): 345-358.
[20] F J Yan, J M Wang, K S Huang. Hybrid electric vehicle model predictive control torque-split strategy incorporating engine transient characteristics. *IEEE Transactions on Vehicular Technology*, 2012, 61(6): 2458-2467.
[21] CT Nguyen, P D Walker, N Zhang. Optimization and coordinated control of gear shift and mode transition for a dual-motor electric vehicle. *Mechanical Systems and Signal Processing*, 2021, 158: 107731.
[22] S Kim, S B Choi. Cooperative control of drive motor and clutch for gear shift of hybrid electric vehicles with dual-clutch transmission. *IEEE/ASME Transactions on Mechatronics,* 2020, 25(3): 1578-1588.
[23] O Atabay, M Ötkür, İ M Ereke. Model based predictive engine torque control for improved drivability. *Proceedings of the Institution of Mechanical Engineers, Part D: Journal of Automobile Engineering*, 2018, 232(12): 1654-1666.
[24] L P Zhang, L Q Yang, X B Guo, et al. Stage-by-phase multivariable combination control for centralized and distributed drive modes switching of electric vehicles. *Mechanism and Machine Theory*, 2020, 147: 10375.
[25] M S Akbari, M H Asemani, N Vafamand, et al. Observer-based predictive control of nonlinear clutchless automated manual transmission for pure electric vehicles: An LPV approach. *IEEE Access*, 2021, 9: 20469-20480.
[26] X M Li, L J Han, H Liu, et al. Real-time optimal energy management strategy for a dual-mode power-split hybrid electric vehicle based on an explicit model predictive control algorithm. *Energy*. 2019, 172: 1161-1178.
[27] Y Yang, Y T Zhang, S Zhang, et al. Control strategy of mode transition with engine start in a plug-in hybrid electric bus. *Energies*, 2019, 12(15): 2989.
[28] X H Zeng, H Y Cui, D F Song, et al. Jerk analysis of a power-split hybrid electric vehicle based on a data-driven vehicle dynamics model. *Energies*, 2018, 11(6): 1537.
[29] W W Mo, J L Wu, P D Walker, et al. Shift characteristics of a bilateral Harpoon-shift synchronizer for electric vehicles equipped with clutchless AMTs. *Mechanical Systems and Signal Processing*, 2021, 148: 107166.
[30] T Pan, H Q Zang, P Wu. Hierarchical mode optimization strategy for gear engagement process of automated manual transmission with electromagnetic actuator. *Proceedings of the Institution of Mechanical Engineers, Part D: Journal of Automobile Engineering*, 2022: 09544070221084434.
[31] Y C Gu. *Gear shift schedule and gearshift control for AMT in hybrid electric vehicle.* Shanghai: Shanghai Jiao Tong University, 2006. (in Chinese).
[32] X Li, K Yu, H Ma, et al. Analysis of varying contact angles and load distributions in defective angular contact ball bearing. *Engineering Failure Analysis,* 2018, 91: 449-464.

Submit your manuscript to a SpringerOpen journal and benefit from:

► Convenient online submission
► Rigorous peer review
► Open access: articles freely available online
► High visibility within the field
► Retaining the copyright to your article

Submit your next manuscript at ► springeropen.com